Eur. Phys. J. C 5, 287–291 (1998)
DOI 10.1007/s100529800847

THE EUROPEAN PHYSICAL JOURNAL C

Relativistic antihydrogen production

H. Meier[1], Z. Halabuka[1], K. Hencken[1], D. Trautmann[1], G. Baur[2]

[1] Institut für Physik der Universität Basel, CH-4056 Basel, Switzerland
[2] Institut für Kernphysik (Theorie), Forschungszentrum Jülich, D-52425 Jülich, Germany

Received: 19 December 1997 / Published online: 10 March 1998

Abstract. Antihydrogen has recently been produced in collisions of antiprotons with ions. While passing through the Coulomb field of a nucleus an antiproton will create an electron-positron pair. In rare cases the positron is bound by the antiproton and an antihydrogen atom produced. We calculate the production of relativistic antihydrogen atoms by bound-free pair production. The cross section is calculated in the semiclassical approximation (SCA), or equivalently in the plane wave Born approximation (PWBA) using exact Dirac-Coulomb wave functions. We compare our calculations to the equivalent photon approximation (EPA).

I Introduction

Antihydrogen, the simplest bound state of antimatter, has first been produced and detected in 1995 at CERN in the Low Energy Antiproton Ring (LEAR) [1]. The synthesis of an antiproton and a positron has been done by passing relativistic antiprotons through a xenon target. Only a few electron-positron pairs are produced in these collisions. In rare cases the velocities of the outgoing positron and antiproton are sufficiently close together, so that the particles join. In lowest order the formalism for calculating the production of antihydrogen is the same as the one used to study bound-free pair production in ion-ion collisions. Bound-free pair production is an important process as it is one of the reactions limiting the luminosity of heavy ion beams in high energy colliders [2]. The equivalent-photon approach (Weizsäcker-Williams method) has been used for the calculations of antihydrogen in [3] and for electron capture by a heavy ions in [4,5]. It is of interest to perform exact calculations in the framework of SCA or, equivalently, PWBA theory and compare them with these calculations, especially at low energies of the colliding particle. The bound-free pair production by bremsstrahlung has been considered in [6] and was found to be negligible. A recent calculation of Baltz shows that contributions of higher order effects reduce the cross section given in lowest order perturbation theory by a small amount for $\gamma \to \infty$ [7].

II Total cross section

The total SCA cross section for pair production with electron capture in a heavy ion collision is given by [8]

$$\sigma_{tot} = 8\pi \left(\frac{Z_P\alpha}{\beta}\right)^2 \int_{m_e}^{\infty} dE_i \int_{q_z}^{\infty} ds \frac{s}{[s^2-(\beta q_z)^2]^2} \times \sum_{\kappa_i} \sum_{m_i,m_f} \left|\left\langle \psi_f(\mathbf{r}) \left| (1-\beta\alpha_3) e^{i\mathbf{qr}} \right| \psi_i(\mathbf{r}) \right\rangle\right|^2 . \quad (1)$$

Throughout the paper we will set $\hbar = c = 1$. The charge numbers of the projectile and target are denoted by Z_P and Z_T; the velocity of the projectile in the target rest frame is given by β. The momentum transfer from projectile to target is $\mathbf{q}$ whose absolute value is given by $s = |\mathbf{q}|$. The component of $\mathbf{q}$ in the direction of the projectile is $q_z = \frac{\omega}{\beta} = \frac{E_f - E_i}{\beta}$. The total energy of the bound electron is E_f; the one of the positron in the continuum $|E_i|$. (Please note that E_i is negative.) The third component of the Dirac matrices is α_3. In our calculation ψ_f $(= \psi_{\kappa_f}^{m_f})$ is the Dirac-Coulomb wave function of a K-shell electron ($\kappa_f = -1$, $E_f = m_e\sqrt{1-\zeta^2}$ with $\zeta = \alpha Z_T$ and magnetic quantum number m_f). ψ_i $(= \psi_{\kappa_i}^{m_i})$ is the wave function of an electron with negative energy E_i in the continuum describing the positron [8].

Because of charge-conjugation invariance the same formalism is used to calculate the production of relativistic antihydrogen in the bound-free process: $\overline{p} + Z_P \to \overline{H}(1s) + Z_P + e^-$.

Using current-conservation we can write (1) as:

$$\sigma_{tot} = 8\pi \left(\frac{Z_P\alpha}{\beta}\right)^2 \int_{m_e}^{\infty} dE_i \int_{q_z}^{\infty} ds\ s \sum_{\kappa_i} \sum_{m_i,m_f} \times \left| \left\langle \psi_f(\mathbf{r}) \left| \left(\frac{1}{s^2} - \frac{\beta_\perp \alpha}{s^2-(\beta q_z)^2} \right) e^{i\mathbf{qr}} \right| \psi_i(\mathbf{r}) \right\rangle \right|^2 . \quad (2)$$

It should be mentioned that (1) and (2) are not exactly equal if the wave functions are not exact eigenfunctions of

the Dirac Hamiltonian [8,9]. The vector $\beta_\perp$ is perpendicular to $\mathbf{q}$ and defined by

$$\beta_\perp = \beta - \left(\beta\frac{\mathbf{q}}{s}\right)\frac{\mathbf{q}}{s} \quad . \tag{3}$$

The solutions of the Dirac equation in the Coulomb field

$$V(r) = -\frac{\zeta}{r}\,, \qquad \zeta = \alpha Z_T \tag{4}$$

are given by [8,10]

$$\psi_\kappa^m = \begin{pmatrix} g_\kappa(r)\chi_\kappa^m(\hat{r}) \\ if_\kappa(r)\chi_{-\kappa}^m(\hat{r}) \end{pmatrix} \quad . \tag{5}$$

The angular dependence is expressed by the spin-angular functions

$$\chi_\kappa^m(\hat{r}) = \sum_{\tau=\pm\frac{1}{2}} (-1)^{l+m-\frac{1}{2}}\sqrt{2j+1} \times \begin{pmatrix} l & \frac{1}{2} & j \\ m-\tau & \tau & -m \end{pmatrix} Y_l^{m-\tau}(\hat{r})\,\chi_\tau \quad . \tag{6}$$

χ_τ are Pauli spinors and

$$j = |\kappa| - \frac{1}{2}\,, \quad l = j + \frac{1}{2}\mathrm{sgn}(\kappa) \quad . \tag{7}$$

The radial functions g_κ and f_κ for the bound state are

$$\begin{pmatrix} g_{-1}(r) \\ f_{-1}(r) \end{pmatrix} = a_0^{-\frac{3}{2}} \frac{(2Z_T)^{\gamma(-1)+\frac{1}{2}}}{[2\Gamma(2\gamma(-1)+1)]^{\frac{1}{2}}} \times \begin{pmatrix} -(1+\gamma(-1))^{\frac{1}{2}} \\ (1-\gamma(-1))^{\frac{1}{2}} \end{pmatrix} \left(\frac{r}{a_0}\right)^{\gamma(-1)-1} e^{-\frac{Z_T r}{a_0}} \tag{8}$$

with the Bohr radius denoted by a_0. For the continuum we use the radial functions

$$\begin{pmatrix} g_{E,\kappa}(r) \\ f_{E,\kappa}(r) \end{pmatrix} = \left(\frac{E+m_e}{E-m_e}\right)^{\frac{1}{4}} \frac{k}{\pi^{\frac{1}{2}}} N\,(kr)^{\gamma(\kappa)-1} \times \begin{pmatrix} \mathrm{Re} \\ \mathrm{sgn}(E)\sqrt{\frac{E-m_e}{E+m_e}}\ \mathrm{Im} \end{pmatrix} \times \left[e^{-i(kr+\phi)}\ {}_1F_1(\gamma(\kappa)+i\eta, 2\gamma(\kappa)+1, 2ikr)\right] \tag{9}$$

which are normalized according to

$$\int_0^\infty dr\ r^2\,[g_{E,\kappa}\,g_{E',\kappa} + f_{E,\kappa}\,f_{E',\kappa}] = \delta(E-E') \quad . \tag{10}$$

In (8) and (9) $\gamma(\kappa)$, k, η and N are given by

$$\gamma(\kappa) = \sqrt{\kappa^2-\zeta^2}, \quad k = \sqrt{E^2-m_e^2}, \quad \eta = \frac{\zeta E}{k},$$
$$N = \frac{2^{\gamma(\kappa)}e^{\frac{\pi\eta}{2}}|\Gamma(\gamma(\kappa)+1+i\eta)|}{\Gamma(2\gamma(\kappa)+1)} \quad . \tag{11}$$

We rewrite the expression in parenthesis in the matrix element of (2) in the spherical basis $(\mathbf{e}_0, \mathbf{e}_{\pm1})$ with $\mathbf{e}_0 = \frac{\mathbf{q}}{s}$ and use the expansion of the vector plane waves into electromagnetic multipoles. From the orthogonality of the spherical harmonics we get the incoherent sum over the multipoles. After some algebra one obtains a relatively simple expression for the cross section.

$$\sigma_{tot}^K = 32\pi^2\left(\frac{Z_P\alpha}{\beta}\right)^2 \int_{m_e}^\infty dE_i \int_{q_z}^\infty ds \times \left\{\frac{T_l}{s^3} + \frac{\beta^2}{2}\frac{s}{[s^2-(\beta q_z)^2]^2}\left(1-\frac{q_z^2}{s^2}\right)T_\perp\right\}\,, \tag{12}$$

with T_l and $T_\perp$ given by

$$T_l = \sum_{\kappa_i,l} \frac{(2j_i+1)(2j_f+1)}{4\pi}(2l+1)\frac{1}{2}\left[1+(-1)^{l_f+l+l_i}\right] \times \left|J^l(E_i,s)\right|^2 \begin{pmatrix} j_f & l & j_i \\ \frac{1}{2} & 0 & -\frac{1}{2} \end{pmatrix}^2 \,, \tag{13}$$

$$T_\perp = \sum_{\kappa_i,l} \frac{(2j_i+1)(2j_f+1)}{4\pi}(2l+1)\Bigg\{\frac{1}{2}\left[1-(-1)^{l_f+l+l_i}\right] \times \frac{1}{l(l+1)}\left|(\kappa_f+\kappa_i)\,I_l^+(E_i,s)\right|^2 + \frac{1}{2}\left[1+(-1)^{l_f+l+l_i}\right]\frac{1}{(2l+1)^2}\Bigg| \left(\frac{l+1}{l}\right)^{\frac{1}{2}} \times \left[(\kappa_f-\kappa_i)\,I_{l-1}^+(E_i,s) - l\ I_{l-1}^-(E_i,s)\right] - \left(\frac{l}{l+1}\right)^{\frac{1}{2}}\left[(\kappa_f-\kappa_i)\,I_{l+1}^+(E_i,s) \times + (l+1)\,I_{l+1}^-(E_i,s)\right]\Bigg|^2\Bigg\} \begin{pmatrix} j_f & l & j_i \\ \frac{1}{2} & 0 & -\frac{1}{2} \end{pmatrix}^2 \quad . \tag{14}$$

The radial integrals are given by

$$J^l(E_i,s) = \int_0^\infty dr\, r^2 j_l(sr) \times [g_{\kappa_f}(r)g_{E_i,\kappa_i}(r) + f_{\kappa_f}(r)f_{E_i,\kappa_i}(r)]\,, \tag{15}$$

$$I_l^\pm(E_i,s) = \int_0^\infty dr\, r^2 j_l(sr) \times [g_{\kappa_f}(r)f_{E_i,\kappa_i}(r) \pm f_{\kappa_f}(r)g_{E_i,\kappa_i}(r)] \tag{16}$$

and are evaluated quickly by the method presented in [11].

III Results

We focus our attention on the process $\overline{p} + Z_P \to \overline{H}(1s) + Z_P + e^-$. In Fig. 1 and Table 1 the total cross section for $Z_P = Z_T = 1$ is given as a function of the Lorentz γ-factor of the projectile in the target rest frame. The cross sections are calculated numerically with (12)–(16).

We compare our results with experimental data measured in the low energy region for La^{57+} target [14]. Our

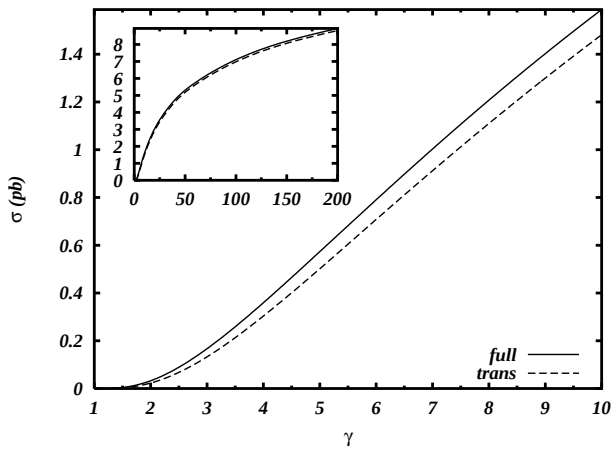

Fig. 1. The *solid line* shows the total cross section σ_{tot}^K for antihydrogen production with a positron bound in the K-shell ($Z_P = Z_T = 1$) as a function of the Lorentz γ-factor of the projectile in the target rest frame. The *dotted line* presents the part of (12) containing $T_\perp$. The cross section scales with Z_P^2

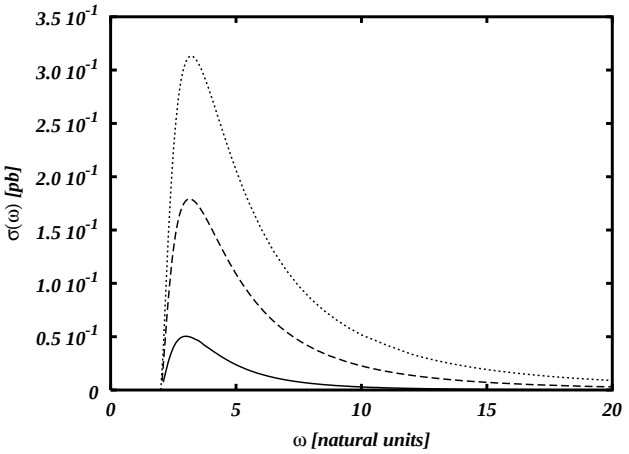

Fig. 2. The cross section for antihydrogen production as a function of ω. The *solid line* shows the cross section for the Lorentz factor $\gamma = 3$ of the projectile in the target rest frame. The *dashed line* shows the cross section for $\gamma = 6$ and the *dotted line* for $\gamma = 10$

Table 1. The total cross section for antihydrogen production ($Z_P = Z_T = 1$) is given for different γ's of the projectile in the target rest frame for the Fermilab experiment [12]. The K-shell capture cross section is denoted by $\overline{H}(1s)$ and the cross section for capture into all shells by $\overline{H}(all)$. The contribution of all higher shells is estimated to 20% of the K capture [5,13]

$\gamma_{target\ rest\ frame}$	$\sigma_{\overline{H}(1s)}$ [pb]	$\sigma_{\overline{H}(all)}$ [pb]
5	$5.73 * 10^{-1}$	$6.88 * 10^{-1}$
6	$7.90 * 10^{-1}$	$9.48 * 10^{-1}$
7	1.00	1.20

calculations for K-shell bound-free pair production of La^{57+} with projectile energies 0.405 GeV/u ($\gamma = 1.43$), 0.956 GeV/u ($\gamma = 2.026$), and 1.3 GeV/u ($\gamma = 2.40$) yields $\sigma^K/Z_P^2 = 9.93 * 10^{-7}$b, $9.12 * 10^{-6}$b, and $1.78 * 10^{-5}$b, respectively. Adding contribution from higher shells, which are assumed to be about 20% [5,13], we find good agreement with the experimental results. We also compare our results with those of Becker [15]. Our results agree well with the results given there for 1 GeV amu^{-1} ($\gamma = 2.07$) and 15 GeV amu^{-1} ($\gamma = 16.1$). Our results for $Z_P = Z_T = 1$ are $\sigma_{tot}^K = 3.92 * 10^{-2}$pb and $\sigma_{tot}^K = 2.55$pb, respectively.

IV Correspondence to EPA

To compare (12) with the photoproduction cross section we rewrite it as:

$$\sigma_{tot}^K = 16\pi^2 \left(\frac{Z_P\alpha}{\beta}\right)^2 \int\limits_{m_e+E_f}^{\infty} d\omega \int\limits_0^{\infty} d(q_\perp^2) \frac{1}{q_\perp^2 + \left(\frac{\omega}{\beta}\right)^2}$$

$$\times \left\{ \frac{1}{q_\perp^2 + \left(\frac{\omega}{\beta}\right)^2} T_l + \frac{\beta^2}{2} \frac{q_\perp^2}{\left[q_\perp^2 + \left(\frac{\omega}{\beta\gamma}\right)^2\right]^2} T_\perp \right\} \quad (17)$$

with $\omega = E_f - E_i$ and $q_\perp^2 = s^2 - q_z^2$; $q_z = \frac{\omega}{\beta}$. σ_{tot}^K as a function of ω is shown in Fig. 2.

The S-matrix element for photo-induced bound-free pair production (also known as photo-induced K-shell capture) in Coulomb gauge is given by

$$S_{fi} = -ie \int_{-\infty}^{\infty} dt \left\langle \psi_f(\mathbf{r}) | \alpha \mathbf{e}_\mu e^{i\mathbf{kr}} | \psi_i(\mathbf{r}) \right\rangle e^{i(E_f - E_i - \omega)t} \quad . \quad (18)$$

Using the multipole expansion for $\mathbf{e}_\mu e^{i\mathbf{kr}}$ we find the expression for the total cross section:

$$\sigma_\gamma^K(\omega) = \frac{8\pi^3\alpha}{\omega} T_\perp(\omega, q^2 = 0) \quad , \quad (19)$$

where $T_\perp$ is the same as in (14), with $s = \omega$. Here we denote the four-momentum of the photon by q. If in (17) T_l is omitted, we can define the photo-induced cross section for 'virtual' photons (see [3] (1)) as

$$\sigma_{\gamma^*}^K(\omega, q^2) = 8\pi^3\alpha \frac{\omega}{q_\perp^2 + \left(\frac{\omega}{\beta}\right)^2} T_\perp(\omega, q^2) \quad . \quad (20)$$

The expression (17) can now be written as $\sigma_{tot}^K(\sigma_{\gamma^*})$. At this stage we can introduce the equivalent photon approximation (EPA). In this approximation the q^2-dependence of $\sigma_{\gamma^*}^K$ is neglected and (20) is replaced by the cross section for real photons (19). Now the integral over $q_\perp$ would diverge and we must introduce a suitable cutoff. Now we can write the cross section in the equivalent photon ap-

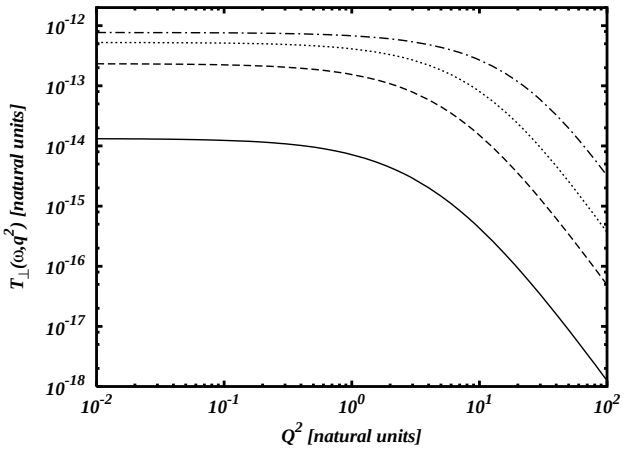

Fig. 3. $T_\perp$ as a function of $Q^2 = -q^2$ for fixed ω-values. The *solid line* shows $T_\perp$ for $\omega = 2.1$, the *dashed line* for $\omega = 3$, the *dotted line* for $\omega = 5$ and the *dash-dotted line* for $\omega = 10$

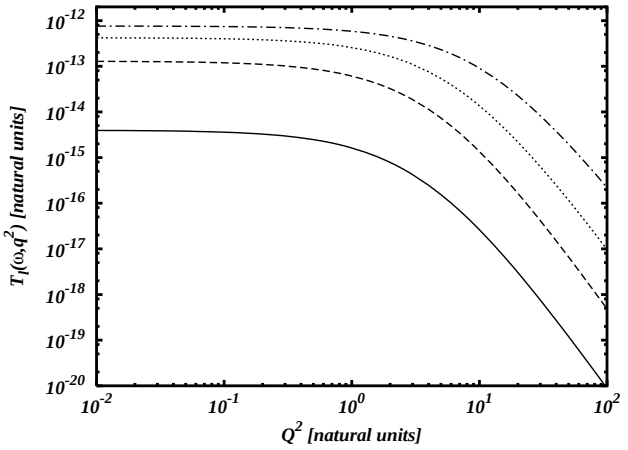

Fig. 4. T_l as a function of Q^2 for fixed ω-values. The *solid line* shows T_l for $\omega = 2.1$, the *dashed line* for $\omega = 3$, the *dotted line* for $\omega = 5$ and the *dash-dotted line* for $\omega = 10$

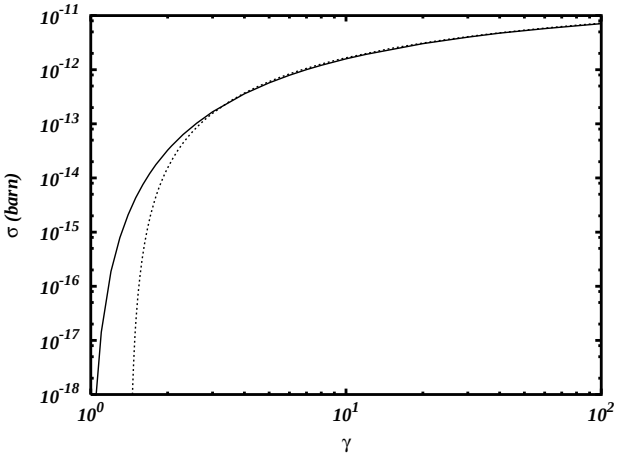

Fig. 5. The *solid line* shows the full SCA calculation results. The *dotted line* shows EPA results with $q^2_{\perp max} = 4m_e^2 - (\frac{\omega}{v\gamma})^2$. For the photo-induced cross section in EPA calculation we used the expression (23)

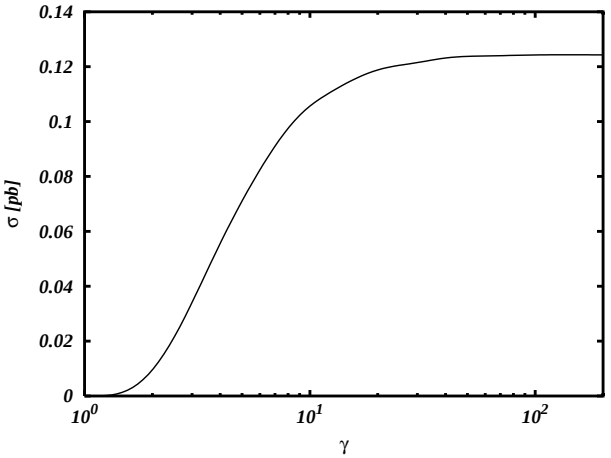

Fig. 6. The *solid line* presents the part of (12) containing T_l

proximation as

$$\sigma^K_{EPA} = \frac{Z_P^2\alpha}{\pi} \int\limits_{m_e+E_f}^{\infty} d\omega \int\limits_0^{q^2_{\perp max}} d(q^2_\perp)\frac{1}{\omega} \times \frac{q^2_\perp}{\left[q^2_\perp + \left(\frac{\omega}{\beta\gamma}\right)^2\right]^2}\,\sigma^K_\gamma(\omega) \quad . \tag{21}$$

$T_\perp(\omega, q^2)$ as a function of the Lorentz-invariant variable $Q^2 = -q^2$ and ω is given in Fig. 3. The momentum $q^2_\perp$ is related to q^2 by

$$q^2 = \omega^2 - q_z^2 - q^2_\perp = -\left(\frac{\omega}{\beta\gamma}\right)^2 - q^2_\perp \quad . \tag{22}$$

From Fig. 3 one can extract the cutoff parameter for the EPA calculation. For the range of ω-values contributing significantly to the total cross section (see Fig. 2) $T_\perp$ is almost constant up to $Q^2_{max} \approx 4m_e^2$. Beyond this value it falls off rapidly. Therefore $q^2_{\perp max}$ is given by $q^2_{max} = Q^2_{max} - (\frac{\omega}{v\gamma})^2$. In Fig. 4 we also show $T_l(\omega, q^2)$ as a function of $Q^2 = -q^2$ and ω which has a similar behavior as $T_\perp$. In Fig. 5 we compare EPA results with the SCA calculation (12).

In the high energy region EPA fits correctly the total cross section. For $\gamma >> 1$, the part of the integral for the total cross section in (12) containing T_l tends to a constant (see Fig. 6). Therefore for high energies of the colliding particles $\sigma_{tot} = \sigma_{EPA} + \sigma_{const}$. For high γ-values we are in agreement with the EPA results of [4,5]. Due to the ω-dependence of the cutoff $q^2_{\perp max} = 4m_e^2 - (\frac{\omega}{v\gamma})^2$ the EPA formula is valid down to $\gamma = 3$. But in the low energy region ($\gamma < 3$) EPA fails. Further for small γ's the contribution of T_l to the total cross section can no longer be neglected but has been ignored in the derivation of the EPA formula (21).

An analytical expression for the photo cross section (19) can be obtained from Sauter's formula for the photo-

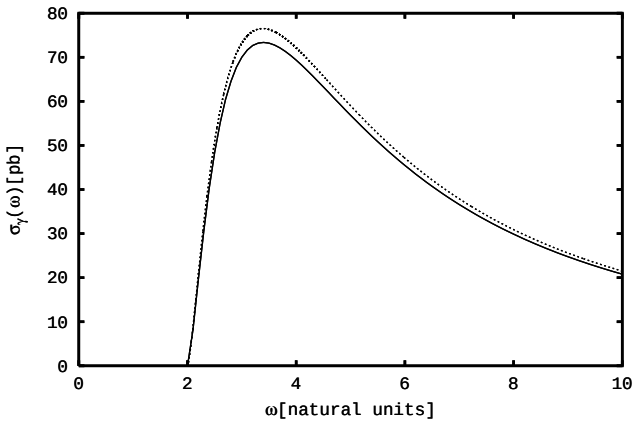

Fig. 7. The *solid line* gives the results of the exact calculations (19) and the *dotted line* the approximated analytical expression (23) for $Z_P = Z_T = 1$

electric effect [16] by means of crossing symmetry:

$$\sigma_\gamma^K = 4\pi\alpha^6 \frac{Z_T^5}{m_e^2}\left[\frac{k_f}{(1-\varepsilon_i)^4} \times \left(\varepsilon_i^2 - \frac{2}{3}\varepsilon_i + \frac{4}{3} - \frac{2-\varepsilon_i}{k_i}\ln(k_i - \varepsilon_i)\right)\right] , \quad (23)$$

with $\varepsilon_i = \frac{E_i}{m_e}$ and $k_i = \sqrt{\varepsilon_i^2 - 1}$. It is an approximation for $\alpha Z_T << 1$ and relativistic velocities of the unbound electron. We compare the exact cross section (19) with the analytic result (23). Very good agreement is expected for $Z_T = 1$. This is shown in Fig. 7. With (19) it is also possible to calculate σ_γ for $\alpha Z_T \sim 1$ where (23) overestimates the cross section (see [4,17]).

V Conclusion

We calculate bound-free pair production in the semiclassical approximation (SCA) using exact Dirac-Coulomb wave functions. We compare results for ion-ion collision with experimental and theoretical data of [4,5,14,15] and find good agreement with their results.

Our calculations have the advantage remaining valid also when the condition $Z\alpha << 1$ is not fulfilled, since exact Dirac wave functions are used. We give expressions for the cross sections already integrated over the angular variables of the free electron (or positron). The radial form factor integrals are evaluated quickly by means of recurrence relations as given in [11]. Therefore we are able to sum over many partial waves and this allows the extension of our calculations up to high values of γ.

We compare the exact results with those of the equivalent photon approximation (EPA). We show that good agreement can be obtained already starting at $\gamma \geq 3$ if one uses an ω-dependent cutoff of $q_{\perp max} = \sqrt{Q_{max}^2 - (\frac{\omega}{\beta\gamma})^2}$ with $Q_{max}^2 \approx 4m_e^2$. This justifies the cutoff chosen in [4,5] at high γ-values. At high energies the contribution of the longitudinal photon tends to a constant. Therefore the total cross section is found to be of the form $\sigma_{tot} = \sigma_{EPA} + \sigma_{const}$.

References

1. PS210 collaboration, W. Oelert, spokesperson, G. Baur et al: Phys. Lett. B **368** (1996) 251
2. S. Datz et al: Nucl. and Instr. Meth. in Phys. Res. B **124** (1997) 129
3. C.T. Munger, S.J. Brodsky, I. Schmidt: Physical Review D **49** (1994) 3228
4. A. Aste, K. Hencken, D. Trautmann, G. Baur: Phys. Rev. A **50** (1994) 3980
5. C.K. Agger, A.H. Sørensen: Phys. Rev. A **55** (1997) 402
6. G. Baur: Phys. Lett. B **311** (1993) 2002
7. A.J. Baltz: Phys. Rev. Lett. **78** (1997) 1231
8. J. Eichler, W.E. Meyerhof: Relativistic Atomic Collisions: Academic Press (1995); J. Eichler: Theory Of Relativistic Ion-Atom Collisons: Physics Reports 193, Nos. 4 & 5 (1990) 165
9. P.A. Amundsen, K. Aashamar: J. Phys. B **14** (1981) 4047
10. M.E. Rose: Relativistic Electron Theory: Wiley, New York (1961)
11. D. Trautmann, G. Baur, F. Rösel: J. Phys. B **16** (1983) 3005
12. M. Mandelkern: letter of intent, experiment E862, Fermilab: available at http://fnphyx-fnal.gov/e862/e862.html
13. C.A. Bertulani, G. Baur: Phys. Rep. **163** (1988) 299
14. A. Belkacem et al: Phys. Rev. Lett. **73** (1994) 2432
15. U. Becker: J. Phys. B **20** (1987) 6563
16. F. Sauter: Ann. Phys. (Leipzig) **11** (1931) 454
17. W.R. Johnson, D.J. Buss, C.O. Carroll: Phys. Rev A **135** (1964) 1232